ACS APPLIED MATERIALS & INTERFACES

Research Article

www.acsami.org

Efficient Hybrid Mesoscopic Solar Cells with Morphology-Controlled $CH_3NH_3PbI_{3-x}Cl_x$ Derived from Two-Step Spin Coating Method

Yuzhuan Xu, Lifeng Zhu, Jiangjian Shi, Songtao Lv, Xin Xu, Junyan Xiao, Juan Dong, Huijue Wu, Yanhong Luo, Dongmei Li,* and Qingbo Meng*

Key Laboratory for Renewable Energy, Chinese Academy of Sciences, Beijing Key Laboratory for New Energy Materials and Devices, Institute of Physics, Chinese Academy of Sciences, Zhongguancun South Third Street 8, Haidian District, Beijing 100190, China

Supporting Information

ABSTRACT: A morphology-controlled $CH_3NH_3PbI_{3-x}Cl_x$ film is synthesized via two-step solution deposition by spin-coating a mixture solution of CH_3NH_3Cl and CH_3NH_3I onto the TiO_2/PbI_2 film for the first time. It is revealed that the existence of CH_3NH_3Cl is supposed to result in a preferential growth along the [110] direction of perovskite, which can improve both the crystallinity and surface coverage of perovskite and reduce the pinholes. Furthermore, the formation process of $CH_3NH_3PbI_{3-x}Cl_x$ perovskite is explored, in which intermediates containing chlorine are suggested to exist. 13.12% of power conversion efficiency has been achieved for the mesoscopic cell, higher than 12.08% of power conversion efficiency of the devices fabricated without CH_3NH_3Cl via the same process. The improvement mainly lies in the increasing open-circuit photovoltage which is ascribed to the reduction of reverse saturation current density.

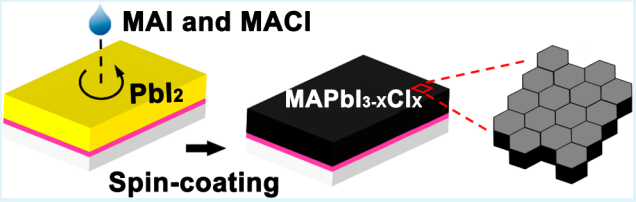

KEYWORDS: *solar cells, mixed-halide lead perovskite, morphology-control, preferential-growth, two-step spin coating, perovskite formation process*

1. INTRODUCTION

Organolead trihalide perovskites are emerging as the most attractive materials in solution-processed, low cost photovoltaic devices, with power conversion efficiencies (PCEs) significantly enhanced from 3.8% to over 19% in 5 years.[1−7] Besides strong light absorption coefficient throughout the UV−vis−NIR spectrum, organolead trihalide perovskites (i.e., $CH_3NH_3PbX_3$) have some outstanding optoelectronic properties, such as high carrier mobility, long charge diffusion length and charge-carrier lifetime, bipolar transport, and so on.[8−13] Typically, the key advantage for perovskite devices over other competing device concepts is that organolead trihalide perovskites are compatible with solution-processing techniques which can promise low fabrication cost.[13]

It is reported that the morphological control is very important to solution-processed planar heterojunction perovskite solar cells.[14] When it comes to the mesostructure perovskite solar cells, the morphology of perovskite capping layer and the crystal structure of perovskite films also play an important role for photovoltaic performances.[15,16] Wang's group investigated the coverage of perovskite capping layers on mesoporous TiO_2 by controlling the concentration of PbI_2 solutions and found the PCE increased with the higher coverages of the perovskite capping layer.[16] They achieved the PCE up to 10.3% by optimizing the perovskite capping layers. Recently, Cheng's group has reported a fully covered and pinhole-free perovskite film consisting of highly crystalline single grains on planar devices by using antisolvent, and the highest PCE of 16.2% has been achieved on planar devices.[17] Obviously, high quality morphology of the perovskite capping layer is one of the key factors for the high efficiency devices. However, it is difficult to fabricate such high quality organolead trihalide perovskite films by the conventional solution approach. Therefore, it is necessary to develop simple new solution-processing techniques to obtain both fully covered and pinhole-free perovskite capping layers.

In this respect, a two-step spin-coating approach has been used to prepare morphology-controlled $CH_3NH_3PbI_{3-x}Cl_x$ perovskite on mesoporous TiO_2 substrates for the first time. We found the $CH_3NH_3PbI_{3-x}Cl_x$ films from this method are pinhole-free and almost full-covered, which permit much easier surface morphology control than the $CH_3NH_3PbI_3$ films under the same spin-coating deposition with only CH_3NH_3I (MAI). The high quality $CH_3NH_3PbI_{3-x}Cl_x$ film allows the fabrication of photovoltaic devices with a PCE up to 13.12% under one sun illumination, in comparison with the $CH_3NH_3PbI_3$ devices fabricated via the same process (12.08%). Moreover, we explored the role of CH_3NH_3Cl (MACl) in the formation process of $CH_3NH_3PbI_{3-x}Cl_x$ perovskite and proved the existence of the intermediates containing chlorine by optical and structural characterizations with this method. It is found that the existence of MACl can lead to a preferential growth along [110] direction of perovskite and significantly enhance the crystallinity of organolead trihalide perovskites, thus leading

Received: September 6, 2014
Accepted: January 14, 2015
Published: January 14, 2015

DOI: 10.1021/am5057807
ACS Appl. Mater. Interfaces 2015, 7, 2242−2248

to a reduction of the defect density of perovskite. All the changes caused by introducing MACl, such as film morphology, crystallinity, coverage, stoichiometry, charge recombination, and defect density, lead to the decreased reverse saturation current density, which finally results in the higher open-circuit photovoltage (V_{oc}). This work offers a considerable insight into the fabrication process of organolead trihalide perovskites as well as the difference between $CH_3NH_3PbI_{3-x}Cl_x$ and $CH_3NH_3PbI_3$ from the view of the perovskite crystal growth process.

2. EXPERIMENTAL SECTION

2.1. Materials. PbI_2 was purchased from Aldrich, dimethylformide (DMF) from Alfar Aesar, and 2,2′,7,7′-tetrakis[*N*,*N*-di(4-methoxyphenyl)amino]-9,9′-spirobifluorene (spiro-MeOTAD) from Luminescence Technology Corp., Taiwan. All of the chemicals were directly used without further purification. CH_3NH_3I and CH_3NH_3Cl were synthesized by following the literature.[18−20] Substrates are fluorine-doped tin oxide conducting glass (FTO, Pilkington, thickness: 2.2 mm, sheet resistance 14 Ω/square). Before use, FTO glass was first washed with mild detergent, rinsed with distilled water for several times and subsequently with ethanol in an ultrasonic bath, and finally dried under air stream.

2.2. Fabrication of the Perovskite Photovoltaic Cells. The 3 cm^2 (1 cm × 3 cm) 50 nm-thickness dense TiO_2 layers were spin-coated on the FTO glass of 6 cm^2 (2 cm × 3 cm) and calcined at 450 °C for 30 min.[20,21] The 500-nm-thickness TiO_2 nanoporous layers (20 nm anatase TiO_2 particles) were subsequently deposited on the dense TiO_2 layer by using screen-printing technique, which were dried at 80 °C for 30 min, then sintered at 450 °C.[22] Before use, the films were immersed into 25 mM $TiCl_4$ at 70 °C for 40 min, and finally sintered at 500 °C for 30 min. The organolead trihalide perovskite layers were obtained by the following steps: first, 1.2 M PbI_2 in DMF was spin-coated onto TiO_2 films at a speed of 3000 rpm for 60 s and heated at 70 °C for several minutes. Also, the transformation from PbI_2 to organolead trihalide perovskites was completed by spin-coating onto the PbI_2 film at a speed of 3000 rpm for 30 s using an isopropanol solution with MAI and MACl in a proper concentration ratio. Then, the films were heated at 95 °C in the air for 40 min. The spiro-MeOTAD layer was subsequently deposited by following the literature.[1] Finally, 80-nm-thickness Au electrode of 0.18 cm^2 (3 mm × 6 mm) was deposited onto the prepared films by thermal evaporation (Kurt J. Lesker) at an atmospheric pressure of 10^{-7} Torr to complete the solar cells.

2.3. Characterizations. The current density−voltage (J−V) characteristics of the cells were recorded on Princeton Applied Research, Model 263, under AM 1.5 irradiation (100 mW/cm^2) from Oriel Solar Simulator 91192. Every J−V curve was measured with 200 data points while the delay time of each point is 100 ms. A black-cardboard mask with a window of 0.08 cm^2 was clipped on the TiO_2 side to define the active area of the cell. The surface morphology and composition of samples were characterized by scanning electron microscope (SEM, FEI XL30 S-FEG). The energy dispersive X-ray (EDX) spectroscopy was obtained on the same instrument. UV−vis absorption spectroscopy was obtained in the range from 400 to 800 nm on UV-2550 spectrophotometer, Shimadzu. X-ray diffraction (XRD) was measured with a Bruker X-ray diffractometer with Cu Kα as the radiation source. The time-resolved photoluminescence (PL) spectroscopy was measured with the PL spectrometer (Edinburgh Instruments, FLS 900) together with a pulsed diode laser (EPL-445, 0.8 μJ/cm^2) at a pulse frequency of 1 MHz. An optical filter at 590 nm was used to filter out the excitation light in the transient PL measurements. The samples for PL measurement were prepared on insulator PMMA (poly(methyl methacrylate)) substrate by two-step spin coating. The thickness of TiO_2 layers was obtained by a surface profiler (KLA-TencorP-6).

3. RESULTS AND DISCUSSION

Two-step spin coating method was first reported to fabricate $CH_3NH_3PbI_3$ for planar devices by Huang'group.[23] Here, we adopt this method to fabricate $CH_3NH_3PbI_3$ and $CH_3NH_3PbI_{3-x}Cl_x$ on mesoporous devices (Scheme 1). Different from the interdiffusion of stacking layers of PbI_2 and MAX (MAI or MAI/MACl) to afford the perovskites in the planar device, the formation of perovskite layer on the mesoporous TiO_2 scaffold is mainly derived from supersaturated MAX solution diffuses into PbI_2 layer and reacts while the isopropanol volatilizing. It must be pointed out that the spin-coating step is right after the solution of MAX dropping onto the PbI_2 film and the XRD pattern of lead iodide disappears after spin-coating, as shown in Figure 1. In other words, the annealing step of perovskite is just a crystal growth process which only improves the crystal quality of perovskites as the relative intensity of perovskite XRD peaks increases (Figure 1).

Scheme 1. Schematic of the Two-Step Spin-Coating Fabricated Process of $CH_3NH_3PbI_{3-x}Cl_x$

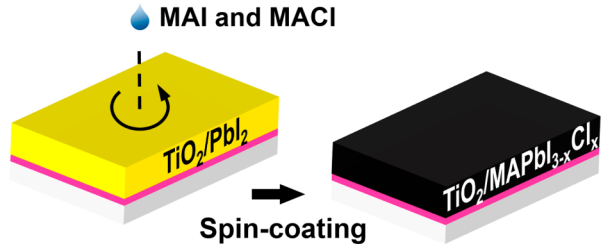

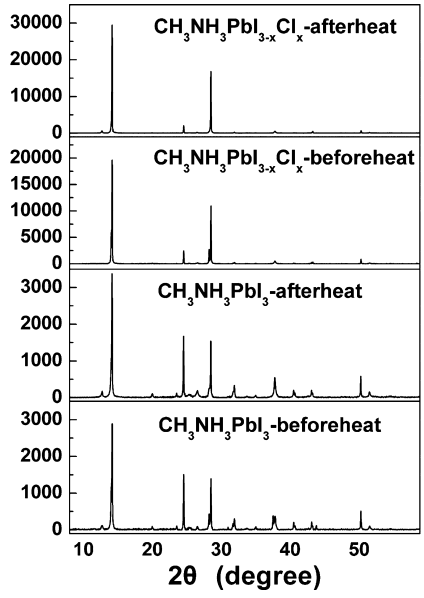

Figure 1. XRD patterns of $CH_3NH_3PbI_{3-x}Cl_x$ film and $CH_3NH_3PbI_3$ film before and after annealing ($CH_3NH_3PbI_3$: 30 mg/mL MAI; $CH_3NH_3PbI_{3-x}Cl_x$: 30 mg/mL MAI and 4 mg/mL MACl).

It is noticed that the relative intensity of the organolead trihalide perovskite peak at about 14.2° (110) greatly increases when MACl is involved (Figure 1), indicating MACl can improve the crystallinity of perovskites. To further study this effect, we examine the XRD patterns of $CH_3NH_3PbI_3$ on mesoporous TiO_2 film prepared from different spin-coating precursor solutions of MAX (Figure 2). It is found that the

DOI: 10.1021/am5057807
ACS Appl. Mater. Interfaces 2015, 7, 2242−2248

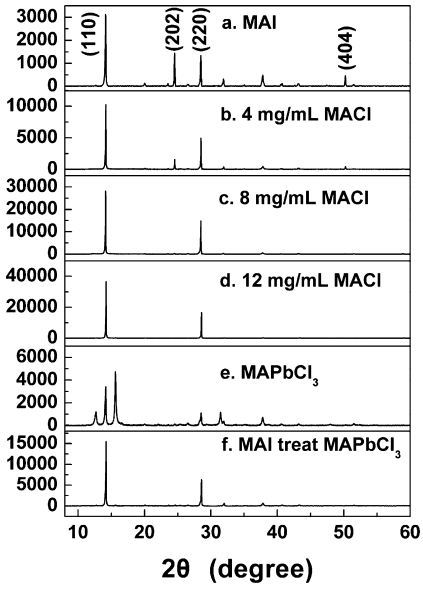

Figure 2. XRD patterns of perovskite films with different spin-coating MAX solutions [(a) 30 mg/mL MAI; (b) 30 mg/mL MAI and 4 mg/mL MACl; (c) 30 mg/mL MAI and 8 mg/mL MACl; (d) 30 mg/mL MAI and 12 mg/mL MACl; (e) 10 mg/mL MAI and 10 mg/mL MACl; (f) 30 mg/mL MAI solution treated the film from part e].

relative intensities of the perovskite peaks at 14.2° (110) and 28.5° (220) are positively correlated with the MACl contents of the MAX solution. Moreover, the peak at 24.5° (202)[19] with the same height as the peak at 28.5° (220) almost disappears as the MACl content increases in the MAX solution. Finally, only the peaks at 14.2° (110) and 28.5° (220) are found in Figure 2d. This suggests the existence of MACl favors the preferential growth direction along the [110] direction which exposes more (110) facet. Since the (110) facet contributes to the long carrier lifetime of perovskites, this change may lead to a longer carrier lifetime.[24]

Figure 3 shows the scanning electron microscopy (SEM) images of the top views of annealed perovskite films prepared from precursor solutions with different composition on mesoporous TiO_2 films (about 500 nm thickness). When no MACl is used, the $CH_3NH_3PbI_3$ perovskite particles are small, and many pinholes can be observed in the films (shown in Figure 3a). By comparison, the $CH_3NH_3PbI_{3-x}Cl_x$ perovskite films are composed of micron-sized grains with almost full surface coverage (shown in Figure 3b). Furthermore, the amounts of the small particles and pinholes decrease as MACl content increases (Supporting Information Figure S1).

In order to further understand the influence of the MACl on the formation of the perovskite, a possible reaction dynamic process is first investigated. According to previous work, the inclusion of MACl can slow down the crystallization of perovskite.[18] Therefore, similar experiments have been designed here. Three identical PbI_2 films were soaked into different MAX isopropanol solutions [(a) 30 mg/mL MAI; (b) a mixed solution of 30 mg/mL MAI and 12 mg/mL MACl; (c) 40 mg/mL MAI] for 5 min at room temperature, then rinsed with isopropanol, and finally were measured by visible light absorption spectroscopy, as seen in Figure 4. Since the PbI_2 films are identical, the different absorptions reflect the different conversion rates of the perovskite in unit time. First, with the MAI concentration increasing (30 to 40 mg/mL), the absorption of the film greatly increases (totally transformed to $CH_3NH_3PbI_3$ for 40 mg/mL), indicating that the reaction rate of transformation from PbI_2 to perovskite is accelerated with the MAI concentration increasing. Second, to the same MAI concentration, the introduction of MACl can increase the

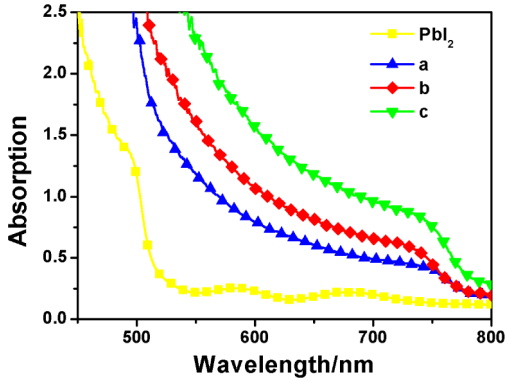

Figure 4. UV−vis spectra of perovskite films formed by immersing them into different MAX isopropanol solution in unit time [(a) 30 mg/mL MAI; (b) 30 mg/mL MAI and 12 mg/mL MACl; (c) 40 mg/mL MAI].

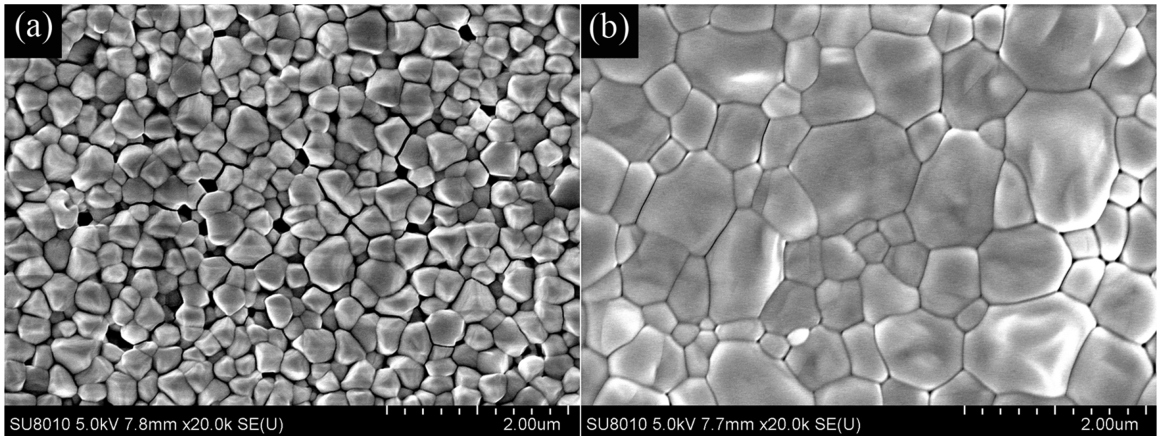

Figure 3. Typical top view SEM images of the annealed organolead trihalide perovskite grown on mesoporous TiO_2 films by two-step spin coating [(a) $CH_3NH_3PbI_3$; (b) $CH_3NH_3PbI_{3-x}Cl_x$)].

DOI: 10.1021/am5057807
ACS Appl. Mater. Interfaces 2015, 7, 2242−2248

absorption; that is, the transformation rate of PbI_2 is also accelerated by the existence of MACl. This seems contrary to the previous work;[18] however, introduction of MACl into the PbI_2/MAI system may cause more complicated reactions (see below), which is supposed to accelerate transformation rate of PbI_2 and decelerate formation rate of perovskite.

Here, in order to further investigate the formation process of $CH_3NH_3PbI_{3-x}Cl_x$ from two-step spin coating method, the microscopic crystal transformation process from PbI_2 to perovskite is considered. PbI_2 crystallizes in the hexagonal CdI_2 structure, in which each Pb atom is coordinated by six I atoms while each I atom is coordinated by three Pb atoms, affording the polyhedral layers of edge-sharing PbI_6 octahedron.[25] The crystal transformation from PbI_2 to $CH_3NH_3PbI_3$ involves the transformation from edge-sharing PbI_6 octahedron to vertex-sharing PbI_6 octahedron and insertion of $CH_3NH_3^+$. Generally, the ionic radius of iodide (206 pm) is larger than that of chloride (167 pm), which may enter into the PbI_2 crystal lattice more readily due to steric hindrance. As a result, some reactive intermediates containing chlorine like $CH_3NH_3PbI_2Cl$ (just a possible one, but we tend to suppose this is the right reactive intermediate in a justifiable process as simple as possible) are suggested during the formation of final $CH_3NH_3PbI_{3-x}Cl_x$ perovskite. Unfortunately, these possible intermediates are too difficult to detect, which are unstable, and the chloride inside will be subsequently replaced by iodide under thermodynamic control. The process from PbI_2 to perovskite will be divided into two parts as follows if the reactive intermediate is $CH_3NH_3PbI_2Cl$:

$$PbI_2 + CH_3NH_3Cl \rightarrow CH_3NH_3PbI_2Cl \quad (1)$$

$$CH_3NH_3PbI_2Cl + CH_3NH_3I \rightarrow CH_3NH_3PbI_3 + CH_3NH_3Cl \quad (2)$$

First, the PbI_2 reacts with MACl to afford $CH_3NH_3PbI_2Cl$. Then, $CH_3NH_3PbI_2Cl$ reacts with MAI to form the $CH_3NH_3PbI_3$ perovskite. Here, the first step accelerates the reaction rate of PbI_2 in the presence of MACl while the second step decelerates the formation rate of final perovskite. A faster first step means a faster nucleation rate of perovskite which leads to a higher surface coverage and a more compacted grain film as the SEM images shown in Figure 3b. Further comparison of two SEM images in Figure 3 reveals that, under the same experimental conditions, large $CH_3NH_3PbI_{3-x}Cl_x$ perovskite grains and some small perovskite grains are obtained while relatively uniform and small $CH_3NH_3PbI_3$ perovskite grains are obtained. These large $CH_3NH_3PbI_{3-x}Cl_x$ perovskite grains are mainly derived from the subsequent Ostwald ripening. A slower second step means a slower crystallization of perovskite which leads to the better crystallinity. According to the EDX results (Supporting Information Figure S2), the content of Cl increases from insignificant 3.46 at. % (which net integration area almost equals its integration error) to significant 7.35 at. % as the content of MACl increases from 4 to 12 mg/mL. This result suggests the following further reactions:

$$CH_3NH_3PbI_2Cl \rightarrow CH_3NH_3PbI_3 + CH_3NH_3PbCl_3 \quad (3)$$

$$CH_3NH_3PbCl_3 + CH_3NH_3I \leftrightarrow CH_3NH_3PbI_3 + CH_3NH_3Cl \quad (4)$$

The eq 4 is a reversible reaction, and a small XRD peak of $MAPbCl_3$ has been found when the content of MACl increases up to 12 mg/mL in the spin-coating solution as shown in the inside XRD patterns of Supporting Information Figure S2. Moreover, this result is in agreement with the idea that the $MAPbI_{3-x}Cl_x$ is a mixture of $MAPbI_3$ and $MAPbCl_3$.[26] Therefore, it is suggested that the slow reversible second step leads to the selective growth of organolead trihalide perovskite which prolongs the crystal growth along the [110] direction and promotes crystallization that contributes to the XRD change.

In terms of the above hypothesis, a competitive equilibrium between iodine and chloride is suggested. That is, if MACl is excess while MAI is not enough, the chloride in the intermediates will be not totally replaced by iodine and may generate a byproduct like $CH_3NH_3PbCl_3$ which belongs to the same space group as $CH_3NH_3PbI_3$.[27] Further experiment is designed to separate the intermediate. When the mixed solution with 10 mg/mL MAI and 10 mg/mL MACl is spin-coated onto the TiO_2/PbI_2 films twice, yellow PbI_2 film turns light grayish brown. By the aid of XRD, it is confirmed that a large amount of $CH_3NH_3PbCl_3$ is formed, as shown in Figure 2e. Subsequently, an isopropanol solution of MAI is spin-coated onto the light grayish brown film, which is converted to the $CH_3NH_3PbI_{3-x}Cl_x$ perovskites finally as expected (Figure 2f).

In order to investigate the effect of the different morphologies of $CH_3NH_3PbI_{3-x}Cl_x$ and $CH_3NH_3PbI_3$ perovskite films on radiative and nonradiative carrier recombination, the time-resolved PL is carried out. The two films are deposited on insulator substrate, and the PL spectra are given in Figure 5a. The data are fitted with two exponential decay curves (here, the longer lifetime was used for comparison) to give the lifetime of carriers.[28] The PL decay lifetime in the $CH_3NH_3PbI_{3-x}Cl_x$ film is 202 ns, longer than that of $CH_3NH_3PbI_3$ film (32 ns), suggesting the defect density reduced which can suppress nonradiative recombination channels.

The current−voltage (J−V) characteristics of the best perovskite solar cells fabricated by spin-coating a mixed isopropanol solution of MAI and MACl or pure MAI isopropanol solution are shown in Figure 5b. Unlike some planar devices,[29] the hysteresis effect in our mesostructure devices is not heavy (Supporting Information Figure S3). Moreover, according to the literature,[30] the stabilized power output under applied bias at the maximum power point approaches that obtained from the negative scan J−V curve (applied bias from open-circuit to short-circuit). Therefore, negative scan curves are adopted here. To the cell using only MAI, an overall PCE of 12.08% is achieved with short-circuit photocurrent density (J_{sc}) of 19.21 mA/cm^2, V_{oc} of 942.2 mV, and fill factor (FF) of 0.67. When MACl is introduced together with MAI, the performance of the perovskite solar cell was increased to 13.12% with the J_{sc} of 18.57 mA/cm^2, V_{oc} of 991 mV, and FF of 0.71. The improvement in the cell performance mainly lies in the increase of V_{oc} and FF compared to the devices without MACl. This improvement can be well-explained with greatly decreased dark current (Figure 5b) caused by the improved perovskite morphology. A classical model of heterojunction solar cell is described as[31−33]

DOI: 10.1021/am5057807
ACS Appl. Mater. Interfaces 2015, 7, 2242−2248

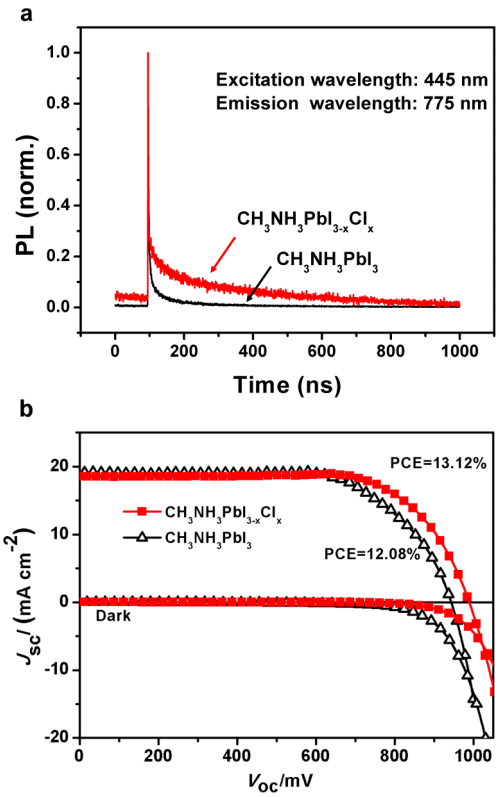

Figure 5. (a) Time-resolved photoluminescence of $CH_3NH_3PbI_3$ and $CH_3NH_3PbI_{3-x}Cl_x$ fabricated by two-step spin-coating on insulator substrate, (b) $J-V$ curve obtained from the best perovskite solar cell fabricated by two-step spin-coating with MACl and without MACl under light irradiation and in the dark.

$$J = J_0\left[\exp\left(\frac{e(V + J \times R_s)}{Ak_BT}\right) - 1\right] + \frac{V + J \times R_s}{R_{sh}} - J_{ph} \quad (5)$$

where J is the recorded current density on the external load, J_0 is the reverse saturation current density of the diode in the dark, e is the elementary charge, V is the applied voltage, k_B is the Boltzmann constant, T is the temperature, J_{ph} is the photogenerated current density, R_s is the series resistance, and R_{sh} is the shunt resistance. By fitting the dark current data with this model we find the ideality factor has little difference between the $CH_3NH_3PbI_3$ device and the $CH_3NH_3PbI_{3-x}Cl_x$ device (both around 2.3) while the J_0 significantly decreases from 6.79×10^{-7} to 2.86×10^{-7} mA/cm^2. V_{oc} could be determined by the formula below:[32]

$$V_{oc} = \frac{Ak_BT}{e}\ln\left(\frac{J_{sc}}{J_0}\right) \quad (6)$$

In eq 6, V_{oc} will increase with J_0 decreasing, which is consistent with the $J-V$ curves under light and dark current measurement. For the ideal solar cells, FF could be determined as[32]

$$FF = \frac{\nu_{oc} - \ln(\nu_{oc} + 0.72)}{\nu_{oc} + 1} \quad (7)$$

where $\nu_{oc} = qV_{oc}/k_BT$. In eq 7, FF will increase with V_{oc} increasing,[34] which is consistent with the $J-V$ curves under light and dark current measurement. It must be pointed out that our devices were all fabricated under the atmosphere except Au electrode deposition. Average $J-V$ data of the top 20 devices of $CH_3NH_3PbI_3$ (Supporting Information Table S1) and $CH_3NH_3PbI_{3-x}Cl_x$ are given in Supporting Information Table S2. From the average performance parameters and the small standard deviation, the high V_{oc} and PCE of $CH_3NH_3PbI_{3-x}Cl_x$ devices are highly reproducible. Moreover, it is found that the content of MACl from 4 mg/mL to 12 mg/mL can give the similar result, while the concentration of MAI is kept at 30 mg/mL under the identical spin-coating method, so the data we present here are all based on 4 mg/mL MACl.

4. CONCLUSION

In conclusion, a two-step solution deposition method by spin-coating a mixture solution of CH_3NH_3Cl and CH_3NH_3I onto the TiO_2/PbI_2 film has been developed to prepare $CH_3NH_3PbI_{3-x}Cl_x$ perovskite films on mesoporous TiO_2 scaffolds for the first time. This two-step spin coating deposition of perovskite permits a considerable morphology control and easy fabrication. Up to 13.12% of PCE has been achieved for $CH_3NH_3PbI_{3-x}Cl_x$-based solar cells. It is found that the introduction of MACl can lead to the preferential growth direction along the [110] direction and significantly enhance the crystallinity. Besides, the defect density of $CH_3NH_3PbI_{3-x}Cl_x$ film is significantly reduced, which can suppress nonradiative recombination channels. The reverse saturation current density is reduced as an overall combined result with MACl introduced, thus leading to a higher V_{oc} compared to the corresponding $CH_3NH_3PbI_3$ perovskite devices. This work provides an insight into the fabrication process of organolead trihalide perovskites and helps us to understand the formation mechanism of the perovskite films. We hope this work can attract attention to the transformation process from PbI_2 to $CH_3NH_3PbI_{3-x}Cl_x$, and we will finally find out the true reactive intermediate in the future. By optimizing the thickness of both perovskite capping layers and mesoporous TiO_2 layers, we expect that a higher efficiency can be achieved, and this part of the research is proceeding in our lab.

■ ASSOCIATED CONTENT

Supporting Information

Extra SEM images and EDX spectra of $CH_3NH_3PbI_{3-x}Cl_x$ fabricated with different CH_3NH_3X (Cl, I) solution. This material is available free of charge via the Internet at http://pubs.acs.org/.

Table 1. Statistical $J-V$ Data of the $CH_3NH_3PbI_3$ and $CH_3NH_3PbI_{3-x}Cl_x$-Based Devices[a]

	J_{sc}/mA cm^2	V_{oc}/mV	FF	PCE/%
$CH_3NH_3PbI_3$ devices	17.50 ± *0.91*	956 ± *18*	0.68 ± *0.02*	11.39 ± *0.37*
$CH_3NH_3PbI_{3-x}Cl_x$ devices	17.76 ± *0.77*	996 ± *23*	0.69 ± *0.03*	12.23 ± *0.42*

[a]The number in the front of each cell is the average value of each data, and the number in italics is the standard deviation of each data. Each data is averaged from 20 devices.

DOI: 10.1021/am5057807
ACS Appl. Mater. Interfaces 2015, 7, 2242−2248

AUTHOR INFORMATION

Corresponding Authors

*E-mail: dmli@iphy.ac.cn.

*E-mail: qbmeng@iphy.ac.cn.

Notes

The authors declare no competing financial interest.

ACKNOWLEDGMENTS

The authors would like to acknowledge the financial support from the NSFC (Nos. 51421002, 51372270, 91433205, 11474333, and 91233202), the MOST (973 Project, Nos. 2012CB932903 and 2012CB932904), and the Knowledge Innovation Program of the Chinese Academy of Sciences. The authors also thank Mr. Yueyong Yang and Ms. Dongfeng Lin for their helpful discussions.

REFERENCES

(1) Liu, M.; Johnston, M. B.; Snaith, H. J. Efficient Planar Heterojunction Perovskite Solar Cells by Vapour Deposition. *Nature* **2013**, *501*, 395−398.

(2) Burschka, J.; Pellet, N.; Moon, S. J.; Humphry-Baker, R.; Gao, P.; Nazeeruddin, M. K.; Grätzel, M. Sequential Deposition as a Route to High-Performance Perovskite-Sensitized Solar Cells. *Nature* **2013**, *499*, 316−319.

(3) Liu, D.; Kelly, T. L. Tunable Lifetime Multiplexing Using Luminescent Nanocrystals. *Nat. Photonics* **2014**, *8*, 32−36.

(4) Jeon, N. J.; Lee, H. G.; Kim, Y. C.; Seo, J.; Noh, J. H.; Lee, J.; Seok, S. I. o-Methoxy Substituents in Spiro-OMeTAD for Efficient Inorganic-Organic Hybrid Perovskite Solar Cells. *J. Am. Chem. Soc.* **2014**, *136*, 7837−7840.

(5) Wang, J. T.-W.; Ball, J. M.; Barea, E. M.; Abate, A.; Alexander-Webber, J. A.; Huang, J.; Saliba, M.; Mora-Sero, I.; Bisquert, J.; Snaith, H. J.; Nicholas, R. J. Low-Temperature Processed Electron Collection Layers of Graphene/TiO_2 Nanocomposites in Thin Film Perovskite Solar Cells. *Nano Lett.* **2014**, *14*, 724−730.

(6) Lee, J.-W.; Seol, D.-J.; Cho, A.-N.; Park, N.-G. High-Efficiency Perovskite Solar Cells Based on the Black Polymorph of $HC(NH_2)_2PbI_3$. *Adv. Mater.* **2014**, *26*, 4991−4998.

(7) Zhou, H.; Chen, Q.; Li, G.; Luo, S.; Song, T.; Duan, H.; Hong, Z.; You, J.; Liu, Y.; Yang, Y. Interface Engineering of Highly Efficient Perovskite Solar Cells. *Science* **2014**, *345*, 542−546.

(8) Xing, G.; Mathews, N.; Sun, S.; Lim, S. S.; Lam, Y. M.; Grätzel, M.; Mhaisalkar, S.; Sum, T. C. Long-Range Balanced Electron- and Hole-Transport Lengths in Organic-Inorganic $CH_3NH_3PbI_3$. *Science* **2013**, *342*, 344−347.

(9) Stranks, S. D.; Eperon, G. E.; Grancini, G.; Menelaou, C.; Alcocer, M. J. P.; Leijtens, T.; Herz, L. M.; Petrozza, A.; Snaith, H. J. Electron-Hole Diffusion Lengths Exceeding 1 Micrometer in an Organometal Trihalide Perovskite Absorber. *Science* **2013**, *342*, 341−344.

(10) Colella, S.; Mosconi, E.; Fedeli, P.; Listorti, A.; Gazza, F.; Orlandi, F.; Ferro, P.; Besagni, T.; Rizzo, A.; Calestani, G.; Gigli, G.; De Angelis, F.; Mosca, R. MAPbI(3-x) Cl-x Mixed Halide Perovskite for Hybrid Solar Cells: The Role of Chloride as Dopant on the Transport and Structural Properties. *Chem. Mater.* **2013**, *25*, 4613−4618.

(11) Hodes, G. Perovskite-Based Solar Cells. *Science* **2013**, *342*, 317−318.

(12) Heo, J. H.; Im, S. H.; Noh, J. H.; Mandal, T. N.; Lim, C.-S.; Chang, J. A.; Lee, Y. H.; Kim, H.-j.; Sarkar, A.; Nazeeruddin, M. K.; Graetzel, M.; Seok, S. I. Efficient Inorganic-Organic Hybrid Heterojunction Solar Cells Containing Perovskite Compound and Polymeric Hole Conductors. *Nat. Photonics* **2013**, *7*, 487−492.

(13) Docampo, P.; Ball, J. M.; Darwich, M.; Eperon, G. E.; Snaith, H. J. Efficient Organometal Trihalide Perovskite Planar-Heterojunction Solar Cells on Flexible Polymer Substrates. *Nat. Commun.* **2013**, *4*, 2761.

(14) Eperon, G. E.; Burlakov, V. M.; Docampo, P.; Goriely, A.; Snaith, H. J. Morphological Control for High Performance, Solution-Processed Planar Heterojunction Perovskite Solar Cells. *Adv. Funct. Mater.* **2014**, *24*, 151−157.

(15) Choi, J. J.; Yang, X.; Norman, Z. M.; Billinge, S. J. L.; Owen, J. S. Structure of Methylammonium Lead Iodide Within Mesoporous Titanium Dioxide: Active Material in High Performance Perovskite Solar Cells. *Nano Lett.* **2014**, *14*, 127−133.

(16) Li, N.; Dong, H.; Dong, H.; Li, J.; Li, W.; Niu, G.; Guo, X.; Wu, Z.; Wang, L. Multifunctional Perovskite Capping Layers in Hybrid Solar Cells. *J. Mater. Chem. A* **2014**, DOI: 10.1039/C4TA02921F.

(17) Xiao, M.; Huang, F.; Huang, W.; Dkhissi, Y.; Zhu, Y.; Etheridge, J.; Gray-Weale, A.; Bach, U.; Cheng, Y.-B.; Spiccia, L. A Fast Deposition-Crystallization Procedure for Highly Efficient Lead Iodide Perovskite Thin-Film Solar Cells. *Angew. Chem.* **2014**, DOI: 10.1002/ange.201405334.

(18) Zhao, Y.; Zhu, K. CH_3NH_3Cl-Assisted One-Step Solution Growth of $CH_3NH_3PbI_3$: Structure, Charge-Carrier Dynamics, and Photovoltaic Properties of Perovskite Solar Cells. *J. Phys. Chem. C* **2014**, *118*, 9412−9418.

(19) Im, J. H.; Lee, C. R.; Lee, J. W.; Park, S. W.; Park, N. G. 6.5% Efficient Perovskite Quantum-Dot-Sensitized Solar Cell. *Nanoscale* **2011**, *3*, 4088−4093.

(20) Lee, M. M.; Teuscher, J.; Miyasaka, T.; Murakami, T. N.; Snaith, H. J. Efficient Hybrid Solar Cells Based on Meso-Superstructured Organometal Halide Perovskites. *Science* **2012**, *338*, 643−647.

(21) Niu, G.; Li, W.; Meng, F.; Wang, L.; Dong, H.; Qiu, Y. Study on the Stability of $CH_3NH_3PbI_3$ Films and the Effect of Post-modification by Aluminum Oxide in All-Solid-State Hybrid Solar Cells. *J. Mater. Chem. A* **2014**, *2*, 705−710.

(22) Li, D.; Wang, M.; Wu, J.; Zhang, Q.; Luo, Y.; Yu, Z.; Meng, Q.; Wu, Z. Application of a New Cyclic Guanidinium Ionic Liquid on Dye-Sensitized Solar Cells (DSCs). *Langmuir* **2009**, *25*, 4808−4814.

(23) Xiao, Z.; Bi, C.; Shao, Y.; Dong, Q.; Wang, Q.; Yuan, Y.; Wang, C.; Gao, Y.; Huang, J. Efficient, High Yield Perovskite Photovoltaic Devices Grown by Interdiffusion of Solution-Processed Precursor Stacking Layers. *Energy Environ. Sci.* **2014**, *7*, 2619−2623.

(24) Haruyama, J.; Sodeyama, K.; Han, L.; Tateyama, Y. Termination Dependence of Tetragonal $CH_3NH_3PbI_3$ Surfaces for Perovskite Solar Cells. *J. Phys. Chem. Lett.* **2014**, *5*, 2903−2909.

(25) Bordas, J.; Robertson, J.; Jakobsson, A. Ultraviolet Properties and Band-Structure of SnS_2, $SnSe_2$, CdI_2, PbI_2, BiI_3 and BiOI Crystals. *J. Phys. C: Solid State Phys.* **1978**, *11*, 2607−2621.

(26) Park, B.; Philippe, B.; Gustafsson, T.; Sveinbjornsson, K.; Hageldt, A.; Johansson, E.; Boschloo, G. Enhanced Crystallinity in Organic-Inorganic Lead Halide Perovskites on Mesoporous TiO_2 via Disorder-Order Phase Transition. *Chem. Mater.* **2014**, *26*, 4466−4471.

(27) Poglitsch, A.; Weber, D. Dynamic Disorder in Methylammoniumtrihalogenoplumbates(II) Observed by Millimeter-Wave Spectroscopy. *J. Chem. Phys.* **1987**, *87*, 6373−6378.

(28) You, J.; Hong, Z.; Yang, Y.; Chen, Q.; Cai, M.; Song, T.-B.; Chen, C.-C.; Lu, S.; Liu, Y.; Zhou, H. Low-Temperature Solution-Processed Perovskite Solar Cells with High Efficiency and Flexibility. *ACS Nano* **2014**, *8*, 1674−1680.

(29) Jeon, N. J.; Noh, J. H.; Kim, Y. C.; Yang, W. S.; Ryu, S., II; Seok, S. Solvent Engineering for High-Performance Inorganic−Organic Hybrid Perovskite Solar Cells. *Nat. Mater.* **2014**, *13*, 897−903.

(30) Snaith, H. J.; Abate, A.; Ball, J. M.; Eperon, G. E.; Leijtens, T.; Noel, N. K.; Stranks, S. D.; Wang, J. T.-W.; Wojciechowski, K.; Zhang, W. Anomalous Hysteresis in Perovskite Solar Cells. *J. Phys. Chem. Lett.* **2014**, *5*, 1511−1515.

(31) Shi, J.; Dong, J.; Lv, S.; Xu, Y.; Zhu, L.; Xiao, J.; Xu, X.; Wu, H.; Li, D.; Luo, Y.; Meng, Q. Hole-Conductor-Free Perovskite Organic Lead Iodide Heterojunction Thin-Film Solar Cells: High Efficiency and Junction Property. *Appl. Phys. Lett.* **2014**, *104*, 063901.

(32) Qi, B.; Wang, J. Fill Factor in Organic Solar Cells. *Phys. Chem. Chem. Phys.* **2013**, *15*, 8972−8982.

(33) Hegedus, S. S.; Shafarman, W. N. Thin-Film Solar Cells: Device Measurements and Analysis. *Prog. Photovoltaics* **2004**, *12*, 155−176.

DOI: 10.1021/am5057807
ACS Appl. Mater. Interfaces 2015, 7, 2242−2248

(34) Devos, A. The Fill Factor of A Solar-Cell From A Mathematical Point of View. *Sol. Cells* **1983**, *8*, 283−296.

DOI: 10.1021/am5057807
ACS Appl. Mater. Interfaces 2015, 7, 2242−2248